Title

Novel Molecular Interactions of Acylcarnitines and Fatty Acids with Myoglobin*

Journal

Journal of Biological Chemistry, 291(48)

ISSN

0021-9258

Authors

Chintapalli, Sree V
Jayanthi, Srinivas
Mallipeddi, Prema L
et al.

Publication Date

2016-11-01

DOI

10.1074/jbc.m116.754978

Peer reviewed

THE JOURNAL OF BIOLOGICAL CHEMISTRY VOL. 291, NO. 48, pp. 25133–25143, November 25, 2016

Novel Molecular Interactions of Acylcarnitines and Fatty Acids with Myoglobin*

Received for publication, August 23, 2016, and in revised form, September 29, 2016 Published, JBC Papers in Press, October 7, 2016, DOI 10.1074/jbc.M116.754978

Sree V. Chintapalli[‡1,2], Srinivas Jayanthi[§1], Prema L. Mallipeddi[¶3], Ravikumar Gundampati[§], Thallapuranam Krishnaswamy Suresh Kumar[§], Damian B. van Rossum[‖], Andriy Anishkin[‡‡], and Sean H. Adams[‡4]**

*From the [‡]Arkansas Children's Nutrition Center and Department of Pediatrics, University of Arkansas for Medical Sciences, Little Rock, Arkansas 72202, the [§]Department of Chemistry and Biochemistry, University of Arkansas, Fayetteville, Arkansas 72701, the [¶]Department of Biology and Biochemistry, University of Houston, Houston, Texas 77204, the [‖]Center for Computational Proteomics and the **Department of Biology, The Pennsylvania State University, University Park, Pennsylvania 16802, and the [‡‡]Department of Biology, University of Maryland, College Park, Maryland 20742*

Edited by George Carman

Previous research has indicated that long-chain fatty acids can bind myoglobin (Mb) in an oxygen-dependent manner. This suggests that oxy-Mb may play an important role in fuel delivery in Mb-rich muscle fibers (*e.g.* type I fibers and cardiomyocytes), and raises the possibility that Mb also serves as an acylcarnitine-binding protein. We report for the first time the putative interaction and affinity characteristics for different chain lengths of both fatty acids and acylcarnitines with oxy-Mb using molecular dynamic simulations and isothermal titration calorimetry experiments. We found that short- to medium-chain fatty acids or acylcarnitines (ranging from C2:0 to C10:0) fail to achieve a stable conformation with oxy-Mb. Furthermore, our results indicate that C12:0 is the minimum chain length essential for stable binding of either fatty acids or acylcarnitines with oxy-Mb. Importantly, the empirical lipid binding studies were consistent with structural modeling. These results reveal that: (i) the lipid binding affinity for oxy-Mb increases as the chain length increases (*i.e.* C12:0 to C18:1), (ii) the binding affinities of acylcarnitines are higher when compared with their respective fatty acid counterparts, and (iii) both fatty acids and acylcarnitines bind to oxy-Mb in 1:1 stoichiometry. Taken together, our results support a model in which oxy-Mb is a novel regulator of long-chain acylcarnitine and fatty acid pools in Mb-rich tissues. This has important implications for physiological fuel management during exercise, and relevance to pathophysiological conditions (*e.g.* fatty acid oxidation disorders and cardiac ischemia) where long-chain acylcarnitine accumulation is evident.

Long-chain fatty acids (LCFAs)[5] serve as an important fuel source for muscle cells, especially Type I "oxidative" muscle fibers and cardiomyocytes (1). Efficient fat combustion requires coincident delivery of fuel and O_2 to mitochondria, with their subsequent metabolic conversions driven by energy demand. On a molecular scale, intracellular trafficking of lipophilic metabolites through a hydrophilic environment presents an interesting problem. Fatty acid-binding proteins (FABPs) have been identified in a variety of cells that solubilize, traffic, and transiently sequester LCFAs (2–8). In this manner, the FABPs help regulate LCFA availability for metabolism and generation of lipid second messengers. Specifically, LCFAs are substrates for acyl-CoA synthetases that activate LCFAs to their CoA esters. These activated moieties flow toward mitochondrial or peroxisomal catabolism, mono-/di-/triacylglycerol synthesis, or metabolism to other derivatives such as ceramides. Acylcarnitines of various chain lengths are formed from a carnitine molecule and their specific fatty acyl-CoA precursors through the actions of acylcarnitine transferases associated with mitochondria and peroxisomes (9).

Importantly, the LCFA availability in muscle can exceed oxidative capacity, and this mismatch, as reflected in plasma or tissue concentrations of acylcarnitine markers of incomplete LCFA β-oxidation, is more apparent during exercise (58) or with insulin resistance and type 2 diabetes (10, 11). Under the latter condition, LCFA accumulation in intramyocellular lipid (IMCL) is evident and IMCL content also correlates with insulin resistance in untrained individuals (12). Interestingly, aerobic training leads to the "athlete's paradox" in which IMCL is increased despite excellent insulin sensitivity in muscle (13). This contrast between trained and untrained individuals is hypothesized to derive from efficient sequestration of fatty acids into triacylglycerol, where they remain relatively "inert," thus limiting accumulation of "lipotoxic" intermediates such as ceramides or diacylgylcerols (14). However, additional possibil-

* This work was supported by U.S. Department of Agriculture, Agricultural Research Service Project 6026-51000-010-05S and support from the Arkansas Children's Research Institute and National Institutes of Health NIDDK Grant R01DK078328-01 (to S. H. A.), pilot award funding from Sturgis Diabetes Research Funds (to S. H. A. and S. V. C.), and Arkansas Bioscience Institute, National Institutes of Health, NCI Grant 1 RO1 CA 172631 (to T. K. S. K.). The authors declare that they have no conflict of interests with the contents of this article. The content is solely the responsibility of the authors and does not necessarily represent the official views of the National Institutes of Health.

[1] Both authors contributed equally to the results of this paper.
[2] To whom correspondence may be addressed: Arkansas Children's Nutrition Center, 15 Children's Way, Little Rock, AR 72202. E-mail: svchintapalli@uams.edu.
[3] Present address: Dept. of Biochemistry, University of Texas Southwestern Medical Center, Dallas, TX 75390.
[4] To whom correspondence may be addressed. E-mail: shadams@uams.edu.

[5] The abbreviations used are: LCFAs, long-chain fatty acids; MD, molecular dynamics; FA, fatty acids; AC, acylcarnitines; ITC, isothermal titration calorimetry; oxy-Mb, oxymyoglobin; Met-Mb, metmyoglobin; deoxy-Mb, deoxymyoglobin; FABP, fatty acid-binding protein; IMCL, intramyocellular lipid; r.m.s. fluctuation, root mean square fluctuation; PLM, palmitate; PLC, palmitoylcarnitine.

ities may be at work including training-associated changes in the expression and/or post-translational modification of sequestration proteins.

Besides being a well-known marker of incomplete β-oxidation, recent studies highlight the multifunctional role that LCFA-acylcarnitines play in the cell. These lipid moieties serve as natural zwitterions that modify membrane-associated systems or enzymes. In turn, these changes can contribute to insulin resistance, inflammation, and myocyte stress responses relevant to cardiac ischemia and inborn errors of fatty acid oxidation (15–17). Despite the importance of acylcarnitines in terms of normal cellular and body-wide fuel metabolism, and their possible involvement in myocellular function (or dysfunction, when in excess), little is known about myocyte acylcarnitine trafficking and sequestration.

Myoglobin (Mb) is a single polypeptide of ~153 amino acids length. Mb is one of the most abundant proteins in muscle and cardiomyocytes (18) and its concentrations in muscle are increased by aerobic training (19). Mb has eight right-handed α-helices that are arranged in a distorted bundle orientation or a triangular prism shape structure (20–22). The arrangement of the protein is highly compact and contains a heme group (*i.e.* porphyrin ring with iron at its center), where the heme is held by a proximal histidine group attached directly to iron. A distal histidine group placed on the opposite side of heme is not bonded to iron; rather, it is involved in binding small molecular ligands (20). The heme is surrounded by the neighboring non-polar amino acids in the interior of the Mb. This compact nature of Mb allows only a few small molecules to reach its interior. Molecular O_2, being non-polar, freely diffuses into the interior of the protein and binds to the heme iron. Binding of O_2 changes the Mb conformation by pulling the iron into the heme plane (*i.e.* in deoxy-Mb the Fe is out of the heme plane). Hence, O_2 binding alters the orientation of the proximal histidine, resulting in a conformational change in the helix F of oxy-Mb.

A growing body of evidence points to Mb as a protein involved in binding LCFAs in an oxygen-dependent manner (23–25). In support, biochemical and NMR studies have demonstrated the *in vitro* interaction between oxy-Mb and palmitate or oleate (26–28). Recently, our group utilized molecular dynamic structural modeling to identify the putative binding site and key amino acid residues involved in fatty acid binding to oxy-Mb, but not deoxy-Mb (23). Although it has been proposed that fatty acid binding to Mb is promoted with unsaturation and increases as a function of chain length (25), the full range of fatty acids bound by oxy-Mb remains to be determined. Nevertheless, these observations raise the intriguing possibility that Mb helps regulate LCFA oxidative *versus* non-oxidative fates under dynamic physiological states (*i.e.* rest *versus* exercise) and/or contrasting metabolic health conditions (*i.e.* fit insulin-sensitive *versus* sedentary insulin-resistant states). In other words, Mb may be an integral part of the network of players that modulate physiologic and lipotoxic outcomes in muscle cells.

Given the LCFA and oxy-Mb interactions, it is reasonable to consider that oxy-Mb may bind acylcarnitines in a chain length-specific manner as well. It is further reasoned that due to the carnitine headgroup, the binding characteristics will differ from LCFA due to polar interactions at the interface between the oxy-Mb hydrophobic pocket and the outside of the protein. To evaluate these hypotheses, we determined the chain length specificity of fatty acid and fatty acylcarnitine binding to oxy-Mb *versus* deoxy-Mb utilizing molecular dynamics (MD) simulations and isothermal titration calorimetry (ITC) experiments. Our findings support a heretofore unrecognized role of Mb in the acylcarnitine pathway and contribute to the understanding of the structural determinants, dynamics, and stability of different chain lengths and ligands with differing unsaturation.

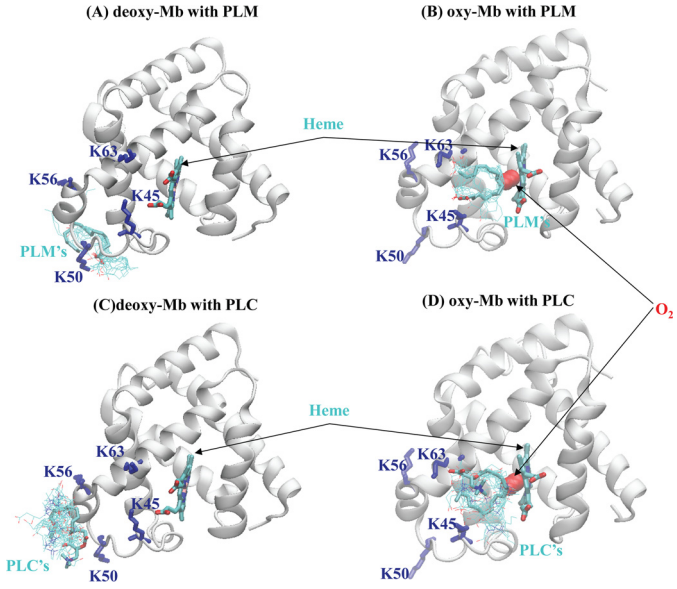

FIGURE 1. **Cluster analysis from AutoDock, displaying docking conformations of horse (*A*) deoxy-Mb with PLM, (*B*) oxy-Mb with PLM, (*C*) deoxy-Mb with PLC, and (*D*) oxy-Mb with PLC.** The best 20 models for PLM and PLC are displayed as *teal-blue lines* and each representative set representative model is displayed as a *stick*. Similar patterns were observed for all the different chain lengths starting from C12 and up to C20, where the ligands for deoxy-Mb are docked close to the lysine residues (*K56* and *K50*) and the ligands for oxy-Mb were placed near the porphyrin ring and the hydrophobic core close to the residues (*K45* and *K63*).

Results

AutoDock Predictions

In our previous study using MD simulations, we showed the mechanistic features predicting the ligand binding site, ligand interactions, and effect(s) of oxygen binding on the heme structure that enables fatty acid binding (*i.e.* palmitate or oleate) to oxy-Mb but not to deoxy-Mb (23). In the current study, we performed molecular docking experiments involving varying chain lengths (C2 to C20) of both fatty acids and acylcarnitines to oxy-Mb and deoxy-Mb.

Docking results for these ligands with deoxy-Mb showed no favorable binding, consistent with previous MD studies and experimental results with LCFAs (23, 27) (Fig. 1, *A* and *C*). This lack of interaction is likely due to the effect of the dome-shaped heme and the degree of heme tilting in deoxy-Mb, which is the result of a slight decrease in the coordination bond length between the iron and histidine (Nϵ2 (ϵ nitrogen of His) and the imidazole ring) (29, 30). For the oxy-Mb simulations, our present results accord with our previous docking outcomes. Both

TABLE 1
Estimated binding energy (BE) results for different chain lengths of both FAs and ACs with oxy-Mb from AutoDock

Length	Name		Estimated BE	
	FAs	ACs	FAs	ACs
			kcal/mol	
C2:0	Acetic	Acetyl	−3.54	−3.77
C4:0	Butyric	Butyroyl	−3.61	−3.81
C6:0	Caproic	Caproyl	−3.72	−3.85
C8:0	Caprylic	Capryloyl	−3.84	−3.93
C10:0	Capric	Caprioyl	−3.90	−4.01
C12:0	Lauric	Lauroyl	−4.52	−5.03
C14:0	Myristic	Myristoyl	−4.75	−5.97
C16:0	Palmitic	Palmitoyl	−5.99	−6.16
C18:1	Oleic	Oleoyl	−6.09	−6.43
C20:4	Arachidonic	Arachidonoyl	−6.81	−7.33

LCFAs and long-chain acylcarnitines exhibit similar binding modes, in that they bind near the porphyrin group and the hydrophobic region of the protein (Fig. 1, *B* and *D*). Specifically, the carboxyl headgroup of the fatty acid or acylcarnitine interacts with the side chain amino group of Lys^{45} and Lys^{63}, whereas the lipid tail region exhibits hydrophobic contacts. Estimated binding energies predicted by Autodock (see Table 1) were lower for the short- and medium-chain fatty acids and their respective acylcarnitines (*i.e.* C2 to C10 values less than −4 kcal/mol), when compared with LCFA and long-chain acylcarnitines. Overall, we found that C2-C10 metabolite binding was not stable (discussed below).

Molecular Dynamic Simulations of the Various Ligands in the Myoglobin Fatty Acid Binding Pocket

Our recent study, using MD simulations of oxy-Mb complexed with palmitate and oleate, illustrated the crucial role of the fatty acid hydrophobic tail in stabilizing the entire protein-lipid complex (23). In the present study, we sought to understand the structural stability of the protein-lipid complex for different chain lengths of ligands as well as the effect of the carnitine headgroup in binding. Therefore, we carried out 100-ns MD simulations separately for each protein-lipid complex (12 fatty acids and 12 acylcarnitines in total). In addition, we also performed simulations using arachidonate or arachidonoylcarnitine (C20:4) to understand the effects of polyunsaturation on binding dynamics, due to the presence of four double bonds. In all cases, the starting structure has the carboxyl group of the lipid interacting with Lys^{45} and Lys^{63} of Mb enabling hydrogen bonding. Analysis of the trajectories for short- and medium-chain acylcarnitines revealed that the ligand starts to move out of the binding site within the first 10-ns simulation time and is thereafter exposed to the hydrophilic environment (Fig. 2, *A–C*, illustrating C4, butyroylcarnitine). Similar outcomes were observed for either fatty acid or acylcarnitine molecules ranging from C2:0 to C10:0 chain length. In other words, there was essentially no binding of either ligand with chain lengths up to C10:0 to oxy-Mb under the conditions tested, as the tail is too short to have stable hydrophobic interactions. For both fatty acids and acylcarnitines, C12:0 is the minimum chain length required to form a stable complex with oxy-Mb (Fig. 3, *A* and *F*).

In our previous studies (23), stable interactions were seen between the non-polar alkyl tail of LCFAs and hydrophobic residues Leu^{29}, Phe^{33}, Phe^{43}, Phe^{46}, Val^{67}, Val^{68}, and Ile^{107} within oxy-Mb. Conversely, the current MD trajectories on short- and medium-chain lipids reveal a failure to exhibit hydrophobic interactions during the course of the simulation run. This is due to the fact that these short tails do not interact with the deeper-sitting hydrophobic residues described above, nor are the interactions strong enough to resist thermal fluctuations and hold the ligands in the hydrophobic groove. Moreover, when a short-tail ligand emerges from the pocket, it lacks a few terminal carbons that would coordinate the tail at the pocket entrance to facilitate the return. Eventually, the short tail region moves far enough out of the pocket, ultimately leading to the dissociation from Mb. This is in sharp contrast with the long-chain lipid moieties in that binding and retention are long lasting. For example, palmitoylcarnitine is stabilized in the hydrophobic pocket, thereby forming hydrogen bonds; its "U"-shaped tail interacts with the conserved hydrophobic residues of Mb (Fig. 2, *D–F*). The energetic reason for the long-chain hydrophobic tail occupying the hydrophobic groove is its highly nonpolar nature, which drives penetration away from the aqueous environment outside of the Mb molecule. In contrast, the fatty tails of short- and medium-chain lipids (C2:0 to C10:0) are not pushed into the crevice because the hydrophobic forces are roughly proportional to the exposed nonpolar area.

In MD simulations, the carboxyl headgroup in LCFA and long-chain acylcarnitines (*i.e.* C12 or longer) exhibited hydrogen-bonding interactions with Lys^{45} or Lys^{63}. The results showed that these headgroups switched between Lys^{45} and Lys^{63} during the 100-ns simulation, with an average dwelling time on the order of 25 ns. During the 100-ns simulations, the majority of the H-bonding is associated with Lys^{45}, with some exceptions (Fig. 4). Overall, we find that the headgroup of fatty acids tend to show a higher percentage of hydrogen bonding with Lys^{45} or Lys^{63} than their respective acylcarnitines (Fig. 4). In addition to this difference, the NH_3^+ moiety in the carnitine headgroup also shows interactions with residues Lys^{42}, Lys^{47}, Ser^{58}, His^{64}, and His^{97}.

Comparative visual analysis of various ligands (C12 and above) in the hydrophobic pocket of oxy-Mb revealed interesting features. Laurate exhibited "linear" shape conformation throughout the 100-ns simulation run, whereas lauroylcarnitine switched between a linear and U-shaped conformation before attaining a final U shape structure (Fig. 3*A*). In contrast, myristate, myristoylcarnitine, palmitate, palmitoylcarnitine, oleate, and oleylcarnitine exhibit the characteristic U-shaped conformation similar to the binding conformation in the FABP proteins (Fig. 3, *panels B–D* and *F–I*) (31–38). Due to the presence of the single double bond at the center of the molecule in both oleate and oleoylcarnitine (formation of kink in the structure due to the *cis* bond between C9 and C10), these two ligands always display U shape conformation. The double-bond limits structural flexibility, which allows the lipids to stabilize the interactions with the surrounding hydrophobic residues. During the MD simulations, the saturated long-chain ligands partially exhibit linear shape during the MD simulations before attaining the final characteristic U shape conformation mimicking LCFAs binding mode in FABPs (31, 32). Long-chain lipids (C14:0 to C18:1) show additional hydrophobic contacts

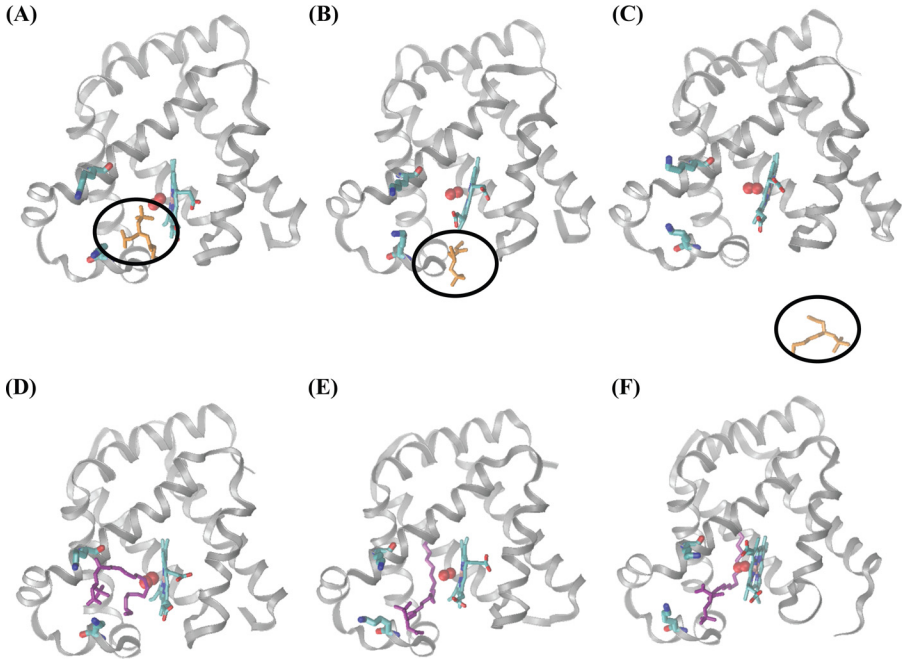

FIGURE 2. **Snapshots of horse oxy-Mb with butyroylcarnitine (*A–C*) and palmitoylcarnitine (*D–F*) over time during MD simulations.** *A,* 0 ns; *B,* 3 ns; and *C,* 6 ns are the time intervals for butyroylcarnitine; and *D,* 0 ns; *E,* 50 ns; and *F,* 100 ns are the time intervals for palmitoylcarnitine. The protein backbone is represented as *ribbon shapes*, whereas butyroylcarnitine (*orange*), palmitoylcarnitine (*purple*), Lys^{45}, Lys^{63}, and heme are displayed as *sticks*. Oxygen molecules are displayed as *red ball shapes* adjacent to the heme moiety. Butyroylcarnitine (*circled*) leaves the binding pocket rapidly, whereas palmitoylcarnitine remains stable in the hydrophobic pocket. Water molecules and ions are excluded for clarity.

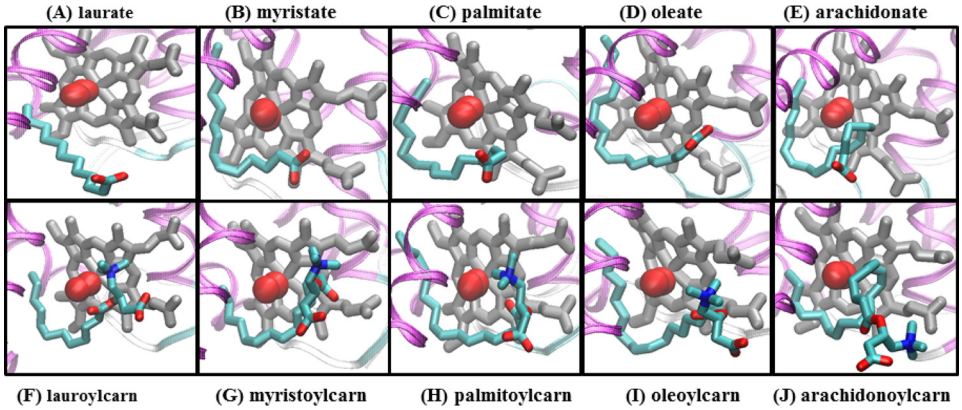

FIGURE 3. **Structure of horse oxy-Mb interacting with fatty acids.** *A,* laurate; *B,* myristate; *C,* palmitate; *D,* oleate; *E,* arachidonate and acylcarnitines; *F,* lauroylcarn; *G,* myristoylcarn; *H,* palmitoylcarn; *I,* oleoylcarn; *J,* arachidonoylcarn. Snapshots of only the fatty acid binding pocket are shown, with various ligands occupying the hydrophobic core near the porphyrin ring. The protein backbone is represented as a *ribbon* (colored *pink*), heme as *sticks* (colored *gray*), and ligands as *sticks* (colored *cyan*). All the ligands appear as the characteristic U-shaped structure, which warps around the oxygen molecule (colored *red*) with the exception of laurate (*A*) having linear and arachidonate (*E*) and arachidonoylcarn (*J*) attaining S-shaped structure.

ranging from Val^{28}, Leu^{29}, Leu^{32}, Phe^{43}, Phe^{46}, Val^{67}, Val^{68}, Ala^{71}, Leu^{72}, Leu^{104}, Ile^{111}, and Leu^{135}. Similar hydrophobic interactions were observed with both arachidonate and arachidonoylcarnitine (C20:4). With respect to the latter, the presence of four *cis* double bonds induces categorical bends in the lipid molecule leading it to attaining an "S"-shaped conformation (Fig. 3, *E* and *J*).

We monitored the stability of the ligands by root mean square fluctuation (r.m.s. fluctuation). We compared the r.m.s. fluctuation trajectories between the 5 fatty acid and 5 acylcarnitine ligands that show stable binding. We found that laurate and lauroylcarnitine ligands exhibited larger movement in the binding pocket when compared with the rest of the lipids tested (Fig. 5). This may be due to the presence of a relatively shorter hydrophobic tail that switches between a linear and U-shaped structure. Fatty acids exhibited lesser movement in the hydrophobic core compared with acylcarnitines. Although their r.m.s. fluctuation profiles are similar (Fig. 5), once the hydrophobic tail occupied the hydrophobic pocket, the carnitine moiety showed larger fluctuations due to the presence of the trimethyl headgroup, which interacts with the surrounding water molecules.

The presence of one *cis* double bond in oleate and oleoylcarnitine and four *cis* double bonds in arachidonate and arachidonoylcarnitine limits the torsional angles of these molecules. The position of the *cis* double bond may also influence the position or the energy cost of bending the tail while docked in the hydrophobic pocket. If the position of the double bonds in the

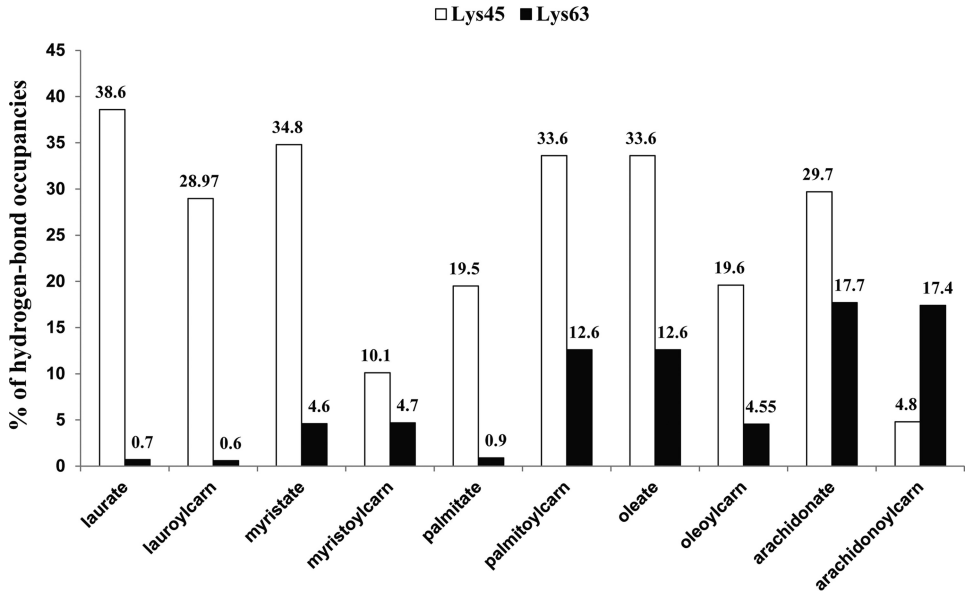

FIGURE 4. **Histograms of percent of hydrogen-bond occupancies for interactions between different ligands with basic residues Lys^{45} and Lys^{63} of horse oxy-Mb, across 100-ns MD simulations.**

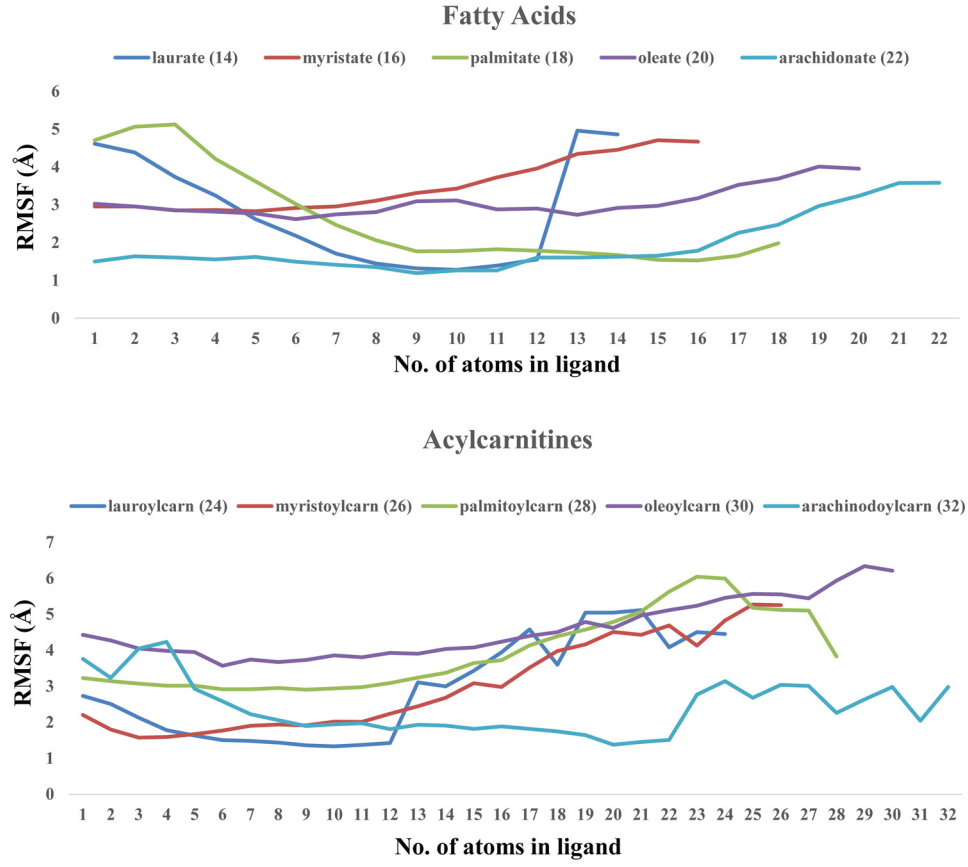

FIGURE 5. **The averaged r.m.s. fluctuation of different fatty acids and acylcarnitines that stably bind oxy-Mb, as a function of time bound to oxy-Mb, showing the deviations by residue.** Only heavy atoms (carbon, oxygen, and nitrogen) are taken into consideration, whereas calculating r.m.s. fluctuations (hydrogens were excluded). Total number of atoms in each ligand molecule; laurate (14), myristate (16), palmitate (18), oleate (20), arachidonate (22), lauroylcarnitine (24), myristoylcarnitine (26), palmitoylcarnitine (28), oleoylcarnitine (30), and arachidonoylcarnitine (32).

lipids changes, the pre-disposed bend might be in the wrong place for the lipid to attain stability. For example, in the case of arachidonoylcarnitine, addition of the carnitine headgroup appears to strengthen the binding by pushing the tail deeper, still exhibiting larger r.m.s. fluctuations, whereas the bend is in different location compared with arachidonate. An opposite scenario is observed in the case of arachidonate and arachidonoylcarnitine as they have fluctuations comparable with both palmitate and palmitoylcarnitine. However, addition of the carnitine headgroup displaces the chain and allows the

arachidonoylcarnitine to fit more optimally. Considering the motion of the ligands, it may be argued that fatty acids and acylcarnitines are not locked in one conformation during the 100-ns simulation, but take on a range of possible conformations before accomplishing a stable conformation in which the tight binding to the protein leads to a stable complex.

The r.m.s. deviations for heme were calculated by aligning the frames of the heme moiety in all the protein-lipid complexes for the whole 100-ns simulation. Analysis of the heme movements (*i.e.* trajectories) in the presence and absence of various lipids revealed an interesting observation. The heme trajectory shows small (<1 Å) r.m.s. deviations throughout the MD simulation, except in a couple of instances where r.m.s. deviations of the heme ring shows larger fluctuations. There was no evidence of large changes in the movement of the heme ring either in the presence or absence of lipid ligands, except for myristate and lauroylcarnitine. However, even small fluctuations in the heme moiety may have a functional role in the release of long-chain lipids, in the process of conversion of oxy-Mb to deoxy-Mb.

Isothermal Titration Calorimetry (ITC)

Optimization of ITC Experimental Conditions and Confirmation of FA and AC Binding to Oxy-Mb—MD simulations support a model in which long-chain ligands exhibit preferential binding to oxy-Mb over deoxy-Mb. We experimentally tested this hypothesis by performing ITC studies. Before conducting the full range of ITC experiments, we assessed different experimental parameters with palmitate (PLM, *i.e.* C16) and Mb. The commercial source of equine myoglobin generally exists in Met-Mb form, which is in ferric (Fe^{3+}) state. Conversion of Met-Mb to Mb was accomplished by the addition of sodium dithionite, which facilitates the reduction of heme iron from ferric (Fe^{3+}) to ferrous (Fe^{2+}) state, thus promoting oxygen binding (25). To increase the percentage of the dissolved oxygen, the Mb solution containing sodium dithionite was further purged with molecular O_2 gas to attain enriched oxy-Mb. For control preparations, deoxy-Mb was generated by purging the Mb preparation with N_2 gas, which eliminates the dissolved oxygen from the solution. Under these conditions, we found a lower binding affinity of PLM to the deoxy-Mb enriched preparation. Specifically, the affinity of PLM for Mb decreased by ~50% (K_d values in μM: N_2 purge, 67.1 ± 3.0 *versus* standard condition, 32.7 ± 1.1 (data not shown)). Comparing standard conditions (*i.e.* sodium dithionite alone) and O_2 purge (*i.e.* sodium dithionite + O_2), we found no significant difference in the PLM K_d values. This notwithstanding, we continued to use the O_2 purge in the follow-up ITC experiments because some ligands may be more sensitive to O_2 concentration than PLM. We also tested the effect of pH and temperature on the affinity of fatty acids or acylcarnitines with Mb. Across the range of pH 6–8 or temperatures 25 to 37 °C, there were no major differences in K_d values between PLM and oxy-Mb (data not shown).

Importantly, the quality of the Met-Mb and oxy-Mb samples was verified by acquiring UV-visual spectra of the samples before and after the ITC experiments. UV-visual spectra of Met-Mb showed the characteristic absorption maxima at 417 nm, and the β and α bands at 504 and 530 nm, respectively. In contrast, oxy-Mb showed significant red shift of the corresponding bands (to 422, 510, and 560 nm, respectively, data not shown). These results are consistent with values reported in the literature for Met-Mb and oxy-Mb-enriched solutions (39).

Having now optimized experimental parameters, we conducted ITC experiments with varied chain lengths of ligands to determine binding to oxy-Mb (enhanced by O_2 purge) *versus* Met-Mb (comprises most of commercial preparations) (Fig. 6). As a negative control, we conducted identical experiments with hen egg white lysozyme, which was titrated independently with palmitate (PLM) and palmitoylcarnitine (PLC) (Fig. 6, *A* and *E*). Lysozyme (~14 kDa) has a similar molecular mass as Mb, and is known to not bind fatty acids. In accord, we found that lysozyme did not exhibit discernable binding to either of the ligands tested. Taken together, these results support the hypothesis that the interaction of LCFAs and long-chain acylcarnitines to oxy-Mb is specific (Fig. 6, *B–D* and *F–H*).

Notably, the variation in the solubility of different fatty acids and acylcarnitines resulted in slight changes in the peaks evolved during the injection process. This is mainly due to the effect of possible aggregation of either fatty acids or acylcarnitines during the titration process, which cannot be accounted for accurately. Nevertheless, appropriate background corrections were performed to eliminate heats of dilution and potential heat changes arising due to products formed during the course of the ITC experiments (see "Experimental Procedures").

Effect of Chain-length of FA and AC on Thermodynamic Binding Parameters of Oxy-Mb—In ITC experiments, fatty acids or acylcarnitines from chain length C6 to C10 showed no significant binding to either Met-Mb or oxy-Mb (Table 2). In contrast, ligands with chain lengths C16:0 and C18:1 showed significant binding to oxy-Mb but not to Met-Mb (Table 2; see Fig. 6 for representative ITC traces). A ~3-fold differential binding affinity was observed in the case of C16:0 and C18:1 fatty acids *versus* acylcarnitines (Table 2). Conversely, C12:0 ligands exhibited very weak binding to oxy-Mb with a K_d value of 509 ± 177 μM (fatty acid) and 864 ± 259 μM (acylcarnitine) due to low heat changes, which may have resulted in an incomplete saturation.

Large negative enthalpic (ΔH) values for both fatty acids and acylcarnitines suggest that the binding interaction to oxy-Mb is favored (Table 2). Observing a decrease in the enthalpy and an increase in the entropy (ΔS) of fatty acids with larger tail length supports the binding of respective ligands to oxy-Mb which is predominantly driven by hydrophobic interactions. Conversely, an opposite trend is observed in acylcarnitines, where an increase in enthalpy and decrease in entropy supports that the interactions are governed by both hydrophobic and hydrogen bonding. On average, all the lipids studied showed a binding stoichiometry of ~1 suggesting the presence of a single, binding site in equine oxy-Mb for either fatty acids or acylcarnitines. The binding affinity of arachidonic acid to oxy-Mb could not be studied due to its poor solubility under the conditions used in the ITC experiment. In addition, experiments

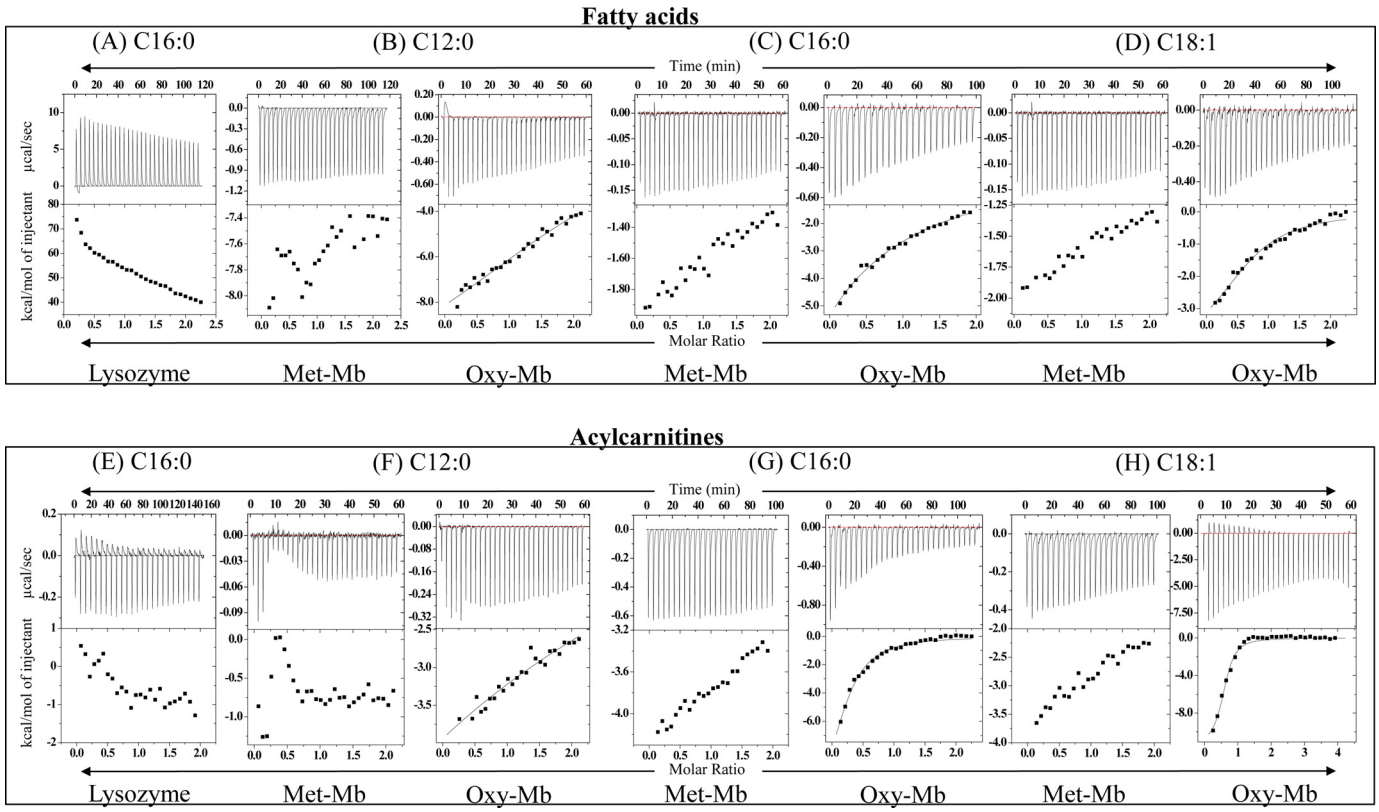

FIGURE 6. **Isothermograms representing the binding of lysozyme, Met-Mb, and oxy-Mb with different chain lengths of fatty acids and acylcarnitines.** Within each metabolite isothermogram, the *upper panel* depicts the raw data of titration of reactants with time in minutes on the *x* axis and the energy releases/absorbed per second on the *y* axis. The *lower panel* is the integrated data with the molar ratio on the *x* axis and energy released/absorbed per injection on the *y* axis. The *solid line* in the *bottom panels* represents the best-fit of the experimental data, using a one-set of sites binding model from MicroCal Origin™.

TABLE 2

Thermodynamic binding parameters of fatty acids and acylcarnitines titrated against Met-Mb or oxy-Mb in ITC experiments

	Samples Chain length	met-Mb Kd (app) µM	oxy-Mb Kd (app) µM	ΔH (kcal·mol^{-1})	ΔS (cal·mol^{-1}·K^{-1})	No. of binding sites
FAs	C6:0	NSB[a]	NSB	NSB	NSB	NSB
	C8:0	NSB	NSB	NSB	NSB	NSB
	C10:0	NSB	NSB	NSB	NSB	NSB
	C12:0	NSB	509 ± 177	-8.01	-12.1	1.6 ± 0.4[b]
	C16:0	NSB	29.1 ± 4.1	-6.81	-2.14	0.76 ± 0.12
	C18:1	NSB	6.17 ± 1.6	-4.33	9.32	0.83 ± 0.42
ACs	C6:0	NSB	NSB	NSB	NSB	NSB
	C8:0	NSB	NSB	NSB	NSB	NSB
	C10:0	NSB	NSB	NSB	NSB	NSB
	C12:0	NSB	864 ± 259	-4.2	-0.07	1.5 ± 0.33[b]
	C16:0	NSB	9.76 ± 2.6	-7.7	-2.9	0.98 ± 0.11
	C18:1	NSB	1.98 ± 0.6	-1.1	-10.8	0.94 ± 0.18

[a] N.S.B., no specific binding detected.
[b] Due to incomplete saturation, the *n* value is greater than 1.

could not be performed with arachidonoylcarnitine as it was not commercially available at the time of the experiments.

Discussion

For both fatty acids and acylcarnitines, ITC data show a consistent strengthening of binding with an increase in the length of the hydrocarbon tail, which agrees with the MD simulations and the expectation that the hydrophobic exclusion of the nonpolar tail from water and its van der Waal interactions with the crevice are crucial factors for the complex stability.

However, there are clear distinctions between fatty acids and acylcarnitines in the enthalpic and entropic contributions to the binding energy, which can be reasonably interpreted in the context of the differences of their headgroup structure. Fatty acids show binding entropy increasing with the tail length. This trend is typical for hydrophobic exclusion as more water gets released from the vicinity of the tail when it enters the Mb crevice. This favorable component is partially balanced by the decreasing favorable enthalpy observed in ITC. For similar systems, the favorable binding enthalpy often comes from strong electrostatic interactions, and its waning in the case of fatty acids is likely due to decrease in the ability of the carboxyl group to engage in polar contacts with the positively charged Mb groups because the larger tail holds it deeper into the Mb crevice and restricts conformational freedom.

In contrast, in the case of acylcarnitine binding, the increase in tail length favors the strengthening of the enthalpic contribution, whereas the unfavorable (negative) entropic part becomes even more pronounced. A possible structural reason for this opposite trend may be due to the headgroups of the lipid moieties. Compared with the small carboxyl in fatty acids, the carnitine headgroup is much larger and heterogeneous in terms of atomic polarity. The carnitine adds both hydrophilic (carboxyl and trimethylammonium) and hydrophobic (two CH2 and one CH) groups to the ligand. It is reasonable to consider that this larger headgroup, with more charged atoms, is able to form more polar contacts with Mb. These interactions may be especially pronounced when a larger lipid tail enforces a deeper placement into the Mb crevice, the situation when the contact abilities of the fatty acid carboxyl are likely to be limited, whereas the larger carnitine headgroup has a farther reach and

more conformational freedom. These differences may contribute to the increase in the enthalpic part of the binding energy with the tail lengthening observed in acylcarnitines. At the same time, several hydrophobic atoms present in the acylcarnitine headgroup might provide a possible "docking spot" for the hydrophobic tail, whereas acyl carnitines are still in the bulk solution. In this case, wrapping of the tail to cover those carbons from water could also limit the size of the hydration shell of the nearby polar atoms in the carnitine headgroup. When acylcarnitines bind to Mb, the tail would unwrap, enter into the Mb crevice and thus expose non-polar carbons of the headgroup to water that would also allow the polar atoms of the headgroup to increase the hydration shell. Typically, hydration of polar atoms makes favorable enthalpic contributions, which would agree with ITC data for acylcarnitines. Additionally, increased hydration of both polar and non-polar atoms in the "uncovered" carnitine headgroup is expected to cause ordering of nearby waters, a likely reason for the larger negative entropy observed with the increased tail length. Hence, affinity of fatty acids and acylcarnitines to oxy-Mb increases with the increase in chain length, whereas the specific energetic contributions and group interactions might differ.

The results from our molecular modeling simulations demonstrate that medium- and long-chain lipids (from C12:0 to C20:4) have the ability to bind oxy-Mb, due to the presence of the long alkyl tail that forms a U- or S-shaped structure occupying the hydrophobic groove of Mb. MD simulations suggest that short- and medium-chain fatty acids and acylcarnitines of C10 or below do not bind to oxy-Mb. Calculated binding energies suggest that acylcarnitines bind relatively more favorably compared with fatty acids because of the presence of the carnitine headgroup. Furthermore, the MD simulations revealed crucial Mb residues Lys^{45} and Lys^{63} anchor the charged end of lipids, whereas hydrophobic residues interact with the hydrophobic tail of the lipid establishing a stable conformation. Consistent results from molecular modeling and ITC studies validate the physical binding of both fatty acids and acylcarnitines to oxy-Mb. Future experiments are warranted to study the mechanism of entry and exit, and to determine the importance of specific residues identified herein (*i.e.* through site-directed mutagenesis). Interestingly, recent studies indicate that oxy-Mb interacts with mitochondria in the muscle cells, initiating a conformational change in the oxy-Mb during the release of oxygen (40, 41). These results must be taken into account in future studies of the retention of fatty acids or acylcarnitines when bound to oxy-Mb that may simultaneously release both oxygen and lipids to the mitochondria.

The novel observation that some acylcarnitines bind to oxy-Mb raises the intriguing possibility that Mb serves as a physiological carrier of fatty acid fuels, especially Mb-rich type I "oxidative" muscle fibers or cardiomyocytes that rely heavily on fatty acid combustion. In addition, MD simulation studies of oxy-Mb with fatty acids and acylcarnitines suggest an important role for these metabolites in the physiological function of the myoglobin as a carrier of oxygen. Indeed, these ligands might stabilize oxygen binding as they partially occlude one of the major oxygen diffusion pathways in Mb. In support, it has been shown that other obstacles can affect the rates of oxygen release (42–44).

Long-chain acylcarnitines can accumulate in muscle: (i) during exercise, (ii) in some fatty acid oxidation disorders, (iii) in the insulin resistant state, and (iv) in cardiac ischemia. Moreover, these metabolites have been hypothesized to serve as bioactive "stress" signals when accumulation is abnormally high (10, 16). It is reasonable to speculate that oxy-Mb impacts the free intracellular concentration of these metabolites, and may be a means by which bioactive acylcarnitines are metered and trafficked in myocytes. Recently, long-chain acylcarnitines were associated with regions of tissue damage in a heart cardiac ischemia model (45). The untoward effects of acylcarnitines on mitochondrial function were ameliorated with addition of total cellular proteins but not FABP or acyl-CoA-binding protein, suggesting the presence of an unknown acylcarnitine-binding protein in cardiomyocytes. Our results suggest that oxy-Mb serves as one such protein. Under conditions of low tissue oxygenation and enrichment of tissue deoxy-Mb (*i.e.* cardiac ischemia), such a model would predict that acylcarnitine binding to Mb drops, thereby raising free intracellular acylcarnitine concentrations with concomitant increases in acylcarnitine-associated cell bioactivities and stress outcomes.

Experimental Procedures

Molecular Docking—We used the identical horse oxy-Mb structure/model coordinates that were previously used to study the PLM and oleate (OLE) interactions with oxy-Mb (23). For horse (*Equus caballus*) deoxy-Mb structure, we used PDB code 2V1K and due to the non-availability of horse oxy-Mb, we transferred the oxygen molecule coordinates from sperm whale oxy-Mb (PDB ID 1MBO) to the deoxy-Mb of horse (46, 47). To attain equilibrium and stability, we performed MD simulations on the generated oxy-Mb complex for a period of 10 ns before using the model for docking studies. All the ligand molecules, which include different fatty acids and acylcarnitines starting from acetic/acetyl- (C2) to arachidonic/arachidonoyl (C-20) were sketched and minimized using Marvin Sketch software (Marvin version 5.7.1, 2011, ChemAxon). The difference between the fatty acid and acylcarnitine is only the addition of carnitine molecule to the headgroup of the fatty acid. Molecular docking was performed using Autodock 4.2 to estimate their binding free energies and to obtain the best orientation of fatty acids and acylcarnitines in oxy-Mb to generate the initial protein-lipid complex for MD simulations (48). A hybrid Lamarckian Genetic Algorithm was used for all the calculations listed in the Autodock module (49). The torsional angles for residues Lys^{45} and Lys^{63}, which are involved in the binding of PLM and oleate, were kept flexible along with the torsional angles of all 24 ligand molecules (48, 50). All the other residues in the oxy-Mb were held rigid. Polar hydrogen atoms were added to the oxy-Mb structure using Autodock and subsequently Kollman united atom partial charges were assigned (48–50). The same input parameters used in our previous study (23) were used for the grid box settings, which is set to $70 \times 70 \times 70$ points with grid spacing of 0.375 Å. Maximum energy evaluations of 25,000,000 steps were performed with a population size of 300,

whereas the total independent runs were fixed to 150. The clustering algorithm described in ADT/AutoDock to group the similar conformation or "clusters" based on their lowest energy conformations and their r.m.s. deviations to one another is applied (48, 50). The docked poses with lowest energy from each run were saved and clustered with an r.m.s. deviation cutoff of 2 Å. Finally, the most energetically favorable conformation of each ligand was selected.

MD Simulations—MD simulations were performed on all of the 24 protein-lipid complexes (12 fatty acids and 12 acylcarnitines) using the NAMD (51) package developed by the Theoretical and Computational Biophysics Group at University of Illinois at Urbana-Champaign (52). All the simulations were conducted using the NPT ensemble using CHARMM36 force field parameters (53, 54). Before performing the MD simulations, the protein-lipid complex was energy minimized for the AutoDock-generated ligand poses. These minimizations used periodic boundary conditions, where the protein-lipid complex was solvated with a TIP3 water model (55) in a rectangular three-dimensional periodic box, of which the dimensions in every direction were chosen to be at least 10 Å larger than the protein-lipid complex. Na^+ and Cl^- ions were added up to equivalent of 150 mM salt concentration to each protein-lipid (oxy-Mb/FA, oxy-Mb/AC) complex to maintain the electroneutrality for all the 24 complexes. Using Langevin dynamics, a constant pressure (1 atm) and temperature regulation (1 to 300 K) with a collision frequency of 1.0 is maintained (56, 57). For the entire MD simulation for each test, periodic boundary settings were maintained with the cutoff distance applied for nonbonded interactions taken as 12 Å, and the particle mesh Ewald method was used to treat long-range electrostatic interactions with the switching distance 1.5 Å. A three-stage protocol was employed for energy minimization of the solvated protein-lipid complex. In the first step, to avoid clashes between conflicting contacts, energy minimization was performed only on the solvent molecules keeping the protein fixed using the steepest descent in the first 3000 steps. In the second step, a conjugate gradient method for 3000 steps was employed keeping the heavy atoms of the oxy-Mb fixed, whereas both the solvent and hydrogen atoms in the oxy-Mb were allowed to relax. In the final step, all the solvent molecules and the protein atoms were allowed to relax for the subsequent 3000 steps during optimization. To achieve equilibrium, the system was subjected to steady heating until it reached 300 K at 1 atm. Throughout the MD simulations, the coordinates of each system were saved every 1 ps. R.m.s. deviation calculations were performed using the plugin r.m.s. deviation trajectory tool, whereas hydrogen bonding interactions of the protein-lipid complex were analyzed using HBonds plugin in vmd 1.9.1 (52).

Isothermal Titration Calorimetry—All the ITC experiments were performed on iTC200 microcalorimeter (GE, Northampton, United Kingdom). Stock solutions of samples containing different chain lengths of free fatty acids and respective acylcarnitines were prepared in 100% ethanol, and diluted to a final concentration of 50 μM in 10 mM sodium phosphate buffer, pH 7.2, containing 50 mM NaCl and 10% ethanol. Incorporation of 10% ethanol in the titration buffer increased the solubility of FAs/ACs at room temperature. At higher concentrations (>500 μM), aggregation was observed in both FAs and ACs. FAs/ACs were always loaded in the reaction cell at a concentration of 50 μM and titrated against 500 μM oxy/Met-Mb solution. Oxy-Mb samples (500 μM) were prepared in the same buffer by the addition of 3 mM sodium dithionite, and O_2 gas was purged into the solution for 10 min. Both the protein and FA/AC samples were equilibrated to 25 °C before the start of the titration. A total of 25 injections (1.6 μl each) from the syringe to cell was carried out to generate the ITC curves within each experiment. Samples were thoroughly mixed by constant stirring of 1000 rpm. Between each injection, a 10 s gap was maintained to achieve a proper baseline. Data obtained from the ITC experiments were best fit to one-set of sites binding model, available on Origin™ software (version 7.0) provided by the manufacturer. Heats of dilutions and heats due to potential products formed during the course of the ITC experiments were corrected by performing appropriate blank titrations, consisting of oxy/Met-Mb into buffer and buffer into FAs/ACs, from the actual sample titrations.

Author Contributions—S. V. C. and S. H. A. conceived the acylcarnitine-Mb binding. S. V. C. conducted all computational experiments, and interpreted MD simulation results in consultation with P. L. M., D. V. R., and A. A. S. J. and R. K. G. conducted ITC experiments and analyzed results with T. K. S. K., S. V. C., S. H. A., T. K. S. K., and S. J. conceived the experimental design. S. V. C. and S. H. A. wrote the manuscript, with input and edits by all authors.

References

1. Randle, P. J. (1998) Regulatory interactions between lipids and carbohydrates: the glucose fatty acid cycle after 35 years. *Diabetes Metab. Rev.* **14,** 263–283
2. Chmurzyńska, A. (2006) The multigene family of fatty acid-binding proteins (FABPs): function, structure and polymorphism. *J. Appl. Genet.* **47,** 39–48
3. Dutta-Roy, A. K. (2000) Cellular uptake of long-chain fatty acids: role of membrane-associated fatty-acid-binding/transport proteins. *Cell Mol. Life Sci.* **57,** 1360–1372
4. Glatz, J. F., and van der Vusse, G. J. (1990) Nomenclature of fatty acid-binding proteins. *Mol. Cell. Biochem.* **98,** 231–235
5. Glatz, J. F., and van der Vusse, G. J. (1990) Cellular fatty acid-binding proteins: current concepts and future directions. *Mol. Cell. Biochem.* **98,** 237–251
6. Ockner, R. K. (1990) Historic overview of studies on fatty acid-binding proteins. *Mol. Cell. Biochem.* **98,** 3–9
7. Kaikaus, R. M., Bass, N. M., and Ockner, R. K. (1990) Functions of fatty acid binding proteins. *Experientia* **46,** 617–630
8. Spener, F., Unterberg, C., Börchers, T., and Grosse, R. (1990) Characteristics of fatty acid-binding proteins and their relation to mammary-derived growth inhibitor. *Mol. Cell Biochem.* **98,** 57–68
9. Sharma, S., and Black, S. M. (2009) Carnitine homeostasis, mitochondrial function, and cardiovascular disease. *Drug Discov. Today Dis. Mech.* **6,** e31–e39
10. Adams, S. H., Hoppel, C. L., Lok, K. H., Zhao, L., Wong, S. W., Minkler, P. E., Hwang, D. H., Newman, J. W., and Garvey, W. T. (2009) Plasma acylcarnitine profiles suggest incomplete long-chain fatty acid beta-oxidation and altered tricarboxylic acid cycle activity in type 2 diabetic African-American women. *J. Nutr.* **139,** 1073–1081
11. Koves, T. R., Ussher, J. R., Noland, R. C., Slentz, D., Mosedale, M., Ilkayeva, O., Bain, J., Stevens, R., Dyck, J. R., Newgard, C. B., Lopaschuk, G. D., and

Muoio, D. M. (2008) Mitochondrial overload and incomplete fatty acid oxidation contribute to skeletal muscle insulin resistance. *Cell Metab.* **7,** 45–56
12. McGarry, J. D. (2002) Banting lecture 2001: dysregulation of fatty acid metabolism in the etiology of type 2 diabetes. *Diabetes* **51,** 7–18
13. Dubé, J. J., Amati, F., Stefanovic-Racic, M., Toledo, F. G., Sauers, S. E., and Goodpaster, B. H. (2008) Exercise-induced alterations in intramyocellular lipids and insulin resistance: the athlete's paradox revisited. *Am. J. Physiol. Endocrinol. Metab.* **294,** E882–888
14. Aon, M. A., Bhatt, N., and Cortassa, S. C. (2014) Mitochondrial and cellular mechanisms for managing lipid excess. *Front. Physiol.* **5,** 282
15. Rutkowsky, J. M., Knotts, T. A., Ono-Moore, K. D., McCoin, C. S., Huang, S., Schneider, D., Singh, S., Adams, S. H., and Hwang, D. H. (2014) Acylcarnitines activate proinflammatory signaling pathways. *Am. J. Physiol. Endocrinol. Metab.* **306,** E1378–1387
16. Aguer, C., McCoin, C. S., Knotts, T. A., Thrush, A. B., Ono-Moore, K., McPherson, R., Dent, R., Hwang, D. H., Adams, S. H., and Harper, M. E. (2015) Acylcarnitines: potential implications for skeletal muscle insulin resistance. *FASEB J.* **29,** 336–345
17. McCoin, C. S., Knotts, T. A., and Adams, S. H. (2015) Acylcarnitines, old actors auditioning for new roles in metabolic physiology. *Nat. Rev. Endocrinol.* **11,** 617–625
18. Nelson, D. (2000) Lehninger Principles of Biochemistry. 3rd Ed., Worth Publishers, New York
19. Terjung, R. L. (1995) Muscle adaptations to aerobic training. *Sports Science Exchange* **8,** 1–4
20. Kendrew, J. C., Bodo, G., Dintzis, H. M., Parrish, R. G., Wyckoff, H., and Phillips, D. C. (1958) A three-dimensional model of the myoglobin molecule obtained by x-ray analysis. *Nature* **181,** 662–666
21. Vinogradov, S. N., Walz, D. A., Pohajdak, B., Moens, L., Kapp, O. H., Suzuki, T., and Trotman, C. N. (1993) Adventitious variability? the amino acid sequences of nonvertebrate globins. *Comp. Biochem. Physiol. B* **106,** 1–26
22. Suzuki, T., and Imai, K. (1998) Evolution of myoglobin. *Cell Mol. Life Sci.* **54,** 979–1004
23. Chintapalli, S. V., Bhardwaj, G., Patel, R., Shah, N., Patterson, R. L., van Rossum, D. B., Anishkin, A., and Adams, S. H. (2015) Molecular dynamic simulations reveal the structural determinants of fatty acid binding to oxy-myoglobin. *PLoS ONE* **10,** e0128496
24. Gloster, J., and Harris, P. (1977) Fatty acid binding to cytoplasmic proteins of myocardium and red and white skeletal muscle in the rat: a possible new role for myoglobin. *Biochem. Biophys. Res. Commun.* **74,** 506–513
25. Götz, F. M., Hertel, M., and Gröschel-Stewart, U. (1994) Fatty acid binding of myoglobin depends on its oxygenation. *Biological chemistry Hoppe-Seyler* **375,** 387–392
26. Sriram, R., Kreutzer, U., Shih, L., and Jue, T. (2008) Interaction of fatty acid with myoglobin. *FEBS Lett.* **582,** 3643–3649
27. Shih, L., Chung, Y., Sriram, R., and Jue, T. (2014) Palmitate interaction with physiological states of myoglobin. *Biochim. Biophys. Acta* **1840,** 656–666
28. Shih, L., Chung, Y., Sriram, R., and Jue, T. (2015) Interaction of myoglobin with oleic acid. *Chem. Phys. Lipids* **191,** 115–122
29. Takano, T. (1977) Structure of myoglobin refined at 2–0 Å resolution: I. crystallographic refinement of metmyoglobin from sperm whale. *J. Mol. Biol.* **110,** 537–568
30. Takano, T. (1977) Structure of myoglobin refined at 2–0 Å resolution: II. structure of deoxymyoglobin from sperm whale. *J. Mol. Biol.* **110,** 569–584
31. He, Y., Yang, X., Wang, H., Estephan, R., Francis, F., Kodukula, S., Storch, J., and Stark, R. E. (2007) Solution-state molecular structure of apo and oleate-liganded liver fatty acid-binding protein. *Biochemistry* **46,** 12543–12556
32. Thompson, J., Winter, N., Terwey, D., Bratt, J., and Banaszak, L. (1997) The crystal structure of the liver fatty acid-binding protein: a complex with two bound oleates. *J. Biol. Chem.* **272,** 7140–7150
33. Lassen, D., Lücke, C., Kveder, M., Mesgarzadeh, A., Schmidt, J. M., Specht, B., Lezius, A., Spener, F., and Rüterjans, H. (1995) Three-dimensional structure of bovine heart fatty-acid-binding protein with bound palmitic acid, determined by multidimensional NMR spectroscopy. *Eur. J. Biochem.* **230,** 266–280
34. Ory, J. J., and Banaszak, L. J. (1999) Studies of the ligand binding reaction of adipocyte lipid binding protein using the fluorescent probe 1,8-anilinonaphthalene-8-sulfonate. *Biophys. J.* **77,** 1107–1116
35. Steele, R. A., Emmert, D. A., Kao, J., Hodsdon, M. E., Frieden, C., and Cistola, D. P. (1998) The three-dimensional structure of a helix-less variant of intestinal fatty acid-binding protein. *Protein Sci.* **7,** 1332–1339
36. Hodsdon, M. E., Ponder, J. W., and Cistola, D. P. (1996) The NMR solution structure of intestinal fatty acid-binding protein complexed with palmitate: application of a novel distance geometry algorithm. *J. Mol. Biol.* **264,** 585–602
37. Zanotti, G., Scapin, G., Spadon, P., Veerkamp, J. H., and Sacchettini, J. C. (1992) Three-dimensional structure of recombinant human muscle fatty acid-binding protein. *J. Biol. Chem.* **267,** 18541–18550
38. Sacchettini, J. C., Gordon, J. I., and Banaszak, L. J. (1989) Refined apoprotein structure of rat intestinal fatty acid binding protein produced in *Escherichia coli*. *Proc. Natl. Acad. Sci. U.S.A.* **86,** 7736–7740
39. Eisert, W. G., Degenkolb, E. O., Noe, L. J., and Rentzepis, P. M. (1979) Kinetics of carboxymyoglobin and oxymyoglobin studied by picosecond spectroscopy. *Biophys. J.* **25,** 455–464
40. Yamada, T., Furuichi, Y., Takakura, H., Hashimoto, T., Hanai, Y., Jue, T., and Masuda, K. (2013) Interaction between myoglobin and mitochondria in rat skeletal muscle. *J. Appl. Physiol.* **114,** 490–497
41. Postnikova, G. B., Tselikova, S. V., and Shekhovtsova, E. A. (2009) Myoglobin and mitochondria: oxymyoglobin interacts with mitochondrial membrane during deoxygenation. *Biochemistry* **74,** 1211–1218
42. Birukou, I., Schweers, R. L., and Olson, J. S. (2010) Distal histidine stabilizes bound O_2 and acts as a gate for ligand entry in both subunits of adult human hemoglobin. *J. Biol. Chem.* **285,** 8840–8854
43. Perutz, M. F., and Mathews, F. S. (1966) An x-ray study of azide methaemoglobin. *J. Mol. Biol.* **21,** 199–202
44. Scott, E. E., Gibson, Q. H., and Olson, J. S. (2001) Mapping the pathways for O_2 entry into and exit from myoglobin. *J. Biol. Chem.* **276,** 5177–5188
45. Liepinsh, E., Makrecka-Kuka, M., Volska, K., Kuka, J., Makarova, E., Antone, U., Sevostjanovs, E., Vilskersts, R., Strods, A., Tars, K., and Dambrova, M. (2016) Long-chain acylcarnitines determine ischaemia/reperfusion-induced damage in heart mitochondria. *Biochem. J.* **473,** 1191–1202
46. Phillips, S. E. (1980) Structure and refinement of oxymyoglobin at 1.6-Å resolution. *J. Mol. Biol.* **142,** 531–554
47. Hersleth, H. P., Uchida, T., Røhr, A. K., Teschner, T., Schünemann, V., Kitagawa, T., Trautwein, A. X., Görbitz, C. H., and Andersson, K. K. (2007) Crystallographic and spectroscopic studies of peroxide-derived myoglobin compound II and occurrence of protonated FeIV O. *J. Biol. Chem.* **282,** 23372–23386
48. Morris, G. M., Huey, R., Lindstrom, W., Sanner, M. F., Belew, R. K., Goodsell, D. S., and Olson, A. J. (2009) AutoDock4 and AutoDockTools4: automated docking with selective receptor flexibility. *J. Comput. Chem.* **30,** 2785–2791
49. Morris, G. M., Goodsell, D. S., Halliday, R. S., Huey, R., Hart, W. E., Belew, R. K., and Olson, A. J. (1998) Automated docking using a Lamarckian genetic algorithm and an empirical binding free energy function. *J. Comput. Chem.* **19,** 1639–1662
50. Goodsell, D. S., Morris, G. M., and Olson, A. J. (1996) Automated docking of flexible ligands: applications of AutoDock. *J. Mol. Recognit.* **9,** 1–5
51. Phillips, J. C., Braun, R., Wang, W., Gumbart, J., Tajkhorshid, E., Villa, E., Chipot, C., Skeel, R. D., Kalé, L., and Schulten, K. (2005) Scalable molecular dynamics with NAMD. *J. Comput. Chem.* **26,** 1781–1802
52. Humphrey, W., Dalke, A., and Schulten, K. (1996) VMD: visual molecular dynamics. *J. Mol. Graph.* **14,** 33–38
53. Klauda, J. B., Venable, R. M., Freites, J. A., O'Connor, J. W., Tobias, D. J., Mondragon-Ramirez, C., Vorobyov, I., MacKerell, A. D., Jr., and

Pastor, R. W. (2010) Update of the CHARMM all-atom additive force field for lipids: validation on six lipid types. *J. Phys. Chem. B* **114,** 7830–7843

54. MacKerell, A. D., Bashford, D. M., Jr., Dunbrack, R. L., Jr., Evanseck, J. D., Field, M. J., Fischer, S., Gao, J., Guo, H., Ha, S., Joseph-McCarthy, D., Kuchnir, L., Kuczera, K., Lau, F. T., Mattos, C., Michnick, S., *et al.* (1998) All-atom empirical potential for molecular modeling and dynamics studies of proteins. *J. Phys. Chem. B* **102,** 3568–3616
55. Jorgensen, W. L., Chandrasekhar, J., Madura, J. D., Impey, R. W., and Klein, M. L. (1983) Comparison of simple potential functions for simulating liquid water. *J. Chem. Phys.* **79,** 926–935
56. Martyna, G. J., Tobias, D. J., and Klein, M. L. (1994) Constant pressure molecular dynamics algorithms. *J. Chem. Phys.* **101,** 4177–4189
57. Feller, S. E., Zhang, Y., Pastor, R. W., and Brooks, B. R. (1995) Constant pressure molecular dynamics simulation: the Langevin piston method. *J. Chem. Phys.* **103,** 4613–4621
58. Zhang, J., Light, A. R., Hoppel, C. L., Campbell, C., Chandler, C. J., Burnett, D. J., Souza, E. C., Casazza, G. A., Hughen, R. W., Keim, N. L., Newman, J. W., Hunter, G. R., Fernandez, J. R., Garvey, W. T., Harper, M. E., *et al.* (2016) Acylcarnitines as markers of exercise-associated fuel partitioning, xenometabolism, and potential signals to muscle afferent neurons. *Exp. Physiol*. 10.1113/EP086019